2006-03

Effects of surface slope on erosion rates of quartz particles

Lodge, Phillip.

UNIVERSITY OF CALIFORNIA

Santa Barbara

Effects of Surface Slope on Erosion Rates of Quartz Particles

A Thesis submitted in partial satisfaction

of the requirements for the degree

Master of Science

In

Mechanical and Environmental Engineering

by

Phillip Lodge

Committee in charge:

Professor Wilbert Lick, Chair

Professor Eric Matthys

Professor Ted Bennett

March 2006

The thesis of Phillip Lodge is approved.

_____

Ted Bennett

_____

Eric Matthys

_____

Wilbert Lick, Committee Chair

February 2006

Effects of Surface Slope on Erosion Rates of Quartz Particles

by

Phillip Lodge

ACKNOWLEDGEMENTS

I wish to acknowledge the patience of everyone involved in this project. After being out of school for ten years, this was the most difficult thing I have ever done. To my wonderful, long-suffering wife, Pearl, and my two daughters, Tanya and Amanda, I give my greatest appreciation for their support and understanding during the long hours that I put into graduate school and the infamous "paper."

Dr. Joe McNeil provided the most time and training towards my efforts in the laboratory, including many hours running experiments. Professor Wilbert Lick provided outstanding academic counseling, education, encouragement, and a great deal of technical assistance. They were truly inspirational to me and I could not have done the project without them.

I will always be grateful for UCSB's financial assistance and to the Navy's graduate school program which permitted me to achieve one of my life's goals. Many thanks to all the folks in the "mud lab." Dr. Rangarajan "Ranga" Sudarsan, Dr. Lijun Jin, and Dr. Tamara Lunsman helped me often with everything from remembering calculus to how to work the laboratory equipment. I'd especially like to thank Professors Ted Bennett and Bud Homsy for their efforts to help me understand fluid mechanics. I will always remember how difficult those courses were and how willing everyone was to help me get through them. I enjoyed my classes with Professors Eric Matthys and Steve McLean and wish to thank them both for their excellent teaching.

ABSTRACT

Effects of Surface Slope on Erosion Rates of Quartz Particles

by Phillip Lodge

Modeling sediment erosion is important in a wide range of environmental problems. Extensive studies of erosion have quantitatively determined the effects on erosion rates of bulk density, particle size, consolidation time, and other parameters, but the effects of surface slope have not been studied. Gravity forces could combine with the shear stresses to enhance erosion.

The effects of surface slope, both in the direction of flow (pitch) and perpendicular to the flow (roll), on erosion rates of quartz particles were investigated using the Sediment Erosion at Depth Flume (Sedflume). Erosion rates were measured for quartz sediments with mean diameters of 5 to 1350-µm, applied shear stresses of 0.4 to 3.2 N/m^2, pitch angles from -30 to +25˚, and roll angles from 0 to 75˚. The sediments consolidated for 3 days (d), 10 d, or 64 d.

For 3-d consolidation time, erosion rates increased for both increasing negative and positive pitch angles. The increase was more rapid as a function of pitch angle for downhill flows than for uphill flows. As particle size decreased below 280-µm, (1) erosion rates decreased and (2) the effect of pitch angle decreased.

Results of 10-d consolidation were qualitatively the same. However, because of longer consolidation time, erosion rates were either the same or lower than for 3-d consolidation.

Roll angle measurements produced qualitatively similar results to those for pitch angle. Consolidation times for roll angle were 3 d for the medium and coarse sediments and 10 d for fine sediments. As particle size decreased below 280-μm, the dependence of erosion rate on roll angle decreased.

Reduced effects on erosion rates as a function of pitch and roll angles as particle size decreased can be explained by cohesive forces that become dominant over gravitational forces as particle size decreases.

Experiments were also conducted by adding 5% of 20-μm quartz to 160-μm quartz. By comparison with 160-μm sediment, which exhibited non-cohesive behavior, the mixed sediment behaved as a cohesive sediment, with roll angle having little effect on erosion rates.

TABLE OF CONTENTS

LIST OF TABLES

LIST OF FIGURES

1 INTRODUCTION

Modeling sediment erosion is important in a wide range of environmental problems, including transport of toxic chemicals in rivers and lakes and scouring around waterside facilities. Sediment erosion has been studied extensively by means of the Sediment Erosion at Depth Flume (Sedflume) (McNeil et al., 1996; Taylor and Lick, 1996; Jepsen et al., 1997; Roberts et al., 1998; Jepsen et al., 1999; Jin et al., 2000). The effects of various environmental factors on erosion rates have been studied, but the effects of surface slope on erosion rates of a wide range of sediments have not been quantified. Surface slope is important when applying the results of studies to sediment beds near shores and riverbanks and near pilings and other structures supporting waterside facilities, because the bed in these areas is generally not flat, gravitational forces could combine with the shear stresses exerted by water flow to enhance erosion. The present research is part of an extensive, on-going investigation of sediment erosion. In this investigation, the effects of various parameters, including bulk density, particle size, mineralogy, time after deposition, and organic content have been studied.

The present investigation emphasizes the effect of surface slope on the erosion rates of quartz particles. Experiments have been done in order to determine the effects of surface slope angle (the angle of the sample's surface with respect to horizontal, both pitch and roll) on the erosion of quartz particles. Uphill flows were considered positive pitch angles, and downhill flows were considered negative pitch angles. Roll angles measured the rotation of the flume around an axis parallel to the

direction of flow. Average particle sizes ranged from 5 to 1350-μm, pitch angles ranged from -30˚ to 25˚, while roll angles ranged from 0˚ to 75˚.

The critical angle, the angle of the bed surface at which the sediment slumps, was measured for several quartz sediments in the general size range used in the erosion experiments.

2 PREVIOUS RESEARCH

As examples of recent and related investigations of erosion rates, measurements have been made of erosion rates and bulk properties of relatively undisturbed sediments from the Detroit River in Michigan, the Lower Fox River in Wisconsin, the Grasse River in New York, the Kalamazoo River in Michigan, Lake Erie, Long Beach Harbor in California, and a dump site offshore of New York Harbor (McNeil et al., 1996; Taylor and Lick, 1996; Jepsen et al., 1997; McNeil et al., 2000). These tests have illustrated the large differences in erosion rates (by as much as several orders of magnitude) at different sites, with depth in the sediments, and as a function of shear stress. In addition, these tests qualitatively determined that erosion rates depend on at least the following parameters: bulk density, particle size (mean and distribution), mineralogy, organic content, salinity of the pore water, amount of gas, oxidation or other chemical reactions, and consolidation time. For the purposes of understanding and accurately predicting erosion rates, the dependence of erosion rates on these parameters needs to be known. This fieldwork also demonstrated that sediment beds

are often sloped. Bed slopes range from near zero in wide, slow-moving estuarine areas to greater than 90° in fast-flowing streams with undercut banks. Sloping sediment beds have a gravitational component of force that may work with the applied shear force of the flow to enhance erosion.

The measurements described above were done using Sedflume, a unique flume that can measure the erosion rates of sediments at high shear stresses (up to stresses on the order of 20 N/m^2) and with depth (down to a meter or more). Although Sedflume was designed and has been used to measure the erosion rates of relatively undisturbed natural sediments from a field site, it can also be used to measure erosion rates of sediments that have been reconstructed in the laboratory to obtain sediments with well-defined properties.

As an example of this, Sedflume has been used with reconstructed sediments to quantitatively determine the effects of bulk density on erosion rates (Jepsen et al., 1997). The sediments used were from the Detroit River, the Lower Fox River, and the Santa Barbara Slough. For each of these sediments and for consolidation times (the time between sample preparation and erosion in Sedflume) varying from 1 to 60 days, the erosion rate as a function of shear stress and depth was measured and related to the local bulk density of the sediment. From these experiments, it was determined that, for each type of sediment (all of which were relatively fine-grained, cohesive sediments), the erosion rate was a unique function of the bulk density and shear stress and could be approximated by

$$E = A\tau^n\rho^m \quad (2.1)$$

where E is the erosion rate (cm/s); τ is the shear stress (N/m^2); ρ is the bulk density (g/cm^3); and A, n, and m are constants that depend on the type of sediment.

In a related set of experiments, the effects of particle size and bulk density on the erosion of quartz particles were investigated (Roberts et al., 1998). Average particle sizes ranged from 5 to 1350 μm, while bulk densities ranged from approximately 1.65 to 1.95 g/cm^3. For the larger particles, the sediments behaved in a non-cohesive manner, i.e., they consolidated rapidly, and the surface eroded particle by particle. For the smaller particles, the sediments behaved in a cohesive manner, i.e., they consolidated relatively slowly, and the surface eroded in particles and chunks. In all cases, erosion rates could be described by Eq. (2.1); they were a very strong decreasing function of density for the finer particles and were essentially independent of density for the larger particles.

An investigation of the effect of adding bentonite (a clay composed primarily of montmorillonite, a member of the smectite family) to sediments has also been made (Jin et al., 2000). In this study, small amounts of bentonite were added to three types of sediment (a topsoil, a sand, and a 50/50 mix of the two). Erosion rates decreased rapidly as the amount of bentonite increased. For example, the addition of 2% bentonite to any of these sediments caused a decrease in erosion rates by one to two orders of magnitude at each shear stress investigated (0.2 to 12.8 N/m^2). The addition

of larger amounts of bentonite caused further decreases in erosion rates, but the decreases decreased as the amount of bentonite increased.

A theoretical description of the initiation of movement of sediments consisting of uniform-size quartz particles has been developed (Gailani, Jin, and Lick, 2004). These sediments behave in a non-cohesive manner for coarse-grained particles, but show cohesive behavior for fine-grained particles, i.e., as the particle size decreases, the critical shear stress , (τ_c), the shear stress "at which the movement of the smallest and easiest-to-erode particles is first noticeable to an observer" (Gailani et al, 2004), increases and also becomes strongly dependent on bulk density. The analysis included gravitational, lift, drag, and cohesive forces, as well as changes in bulk density; it is uniformly valid for the range of particle sizes investigated, from fine-grained, cohesive particles to coarse-grained, non-cohesive particles.

From theory and experiments, it was shown that the gravitational force was given by

$$F_g = c_3 d^3 \tag{2.2}$$

while the cohesive force was given by

$$F_c = c_4 d \tag{2.3}$$

The coefficients c_3 and c_4 are given approximately by 8.21×10^3 N/m^3 and 1.33×10^{-4} N/m, respectively. These forces are shown as a function of particle diameter in Fig. 2.1.

Approximate equations to describe the dependence of sediment erosion rates on the applied shear stress, the critical shear stress for erosion, and the critical shear stress for erosion of non-cohesive sediments have been developed and compared with experiment (Gailani et al., 2004). Equations for erosion rates of natural sediments are presented which are (a) valid for fine-grained, cohesive sediments, (b) valid for coarse-grained, non-cohesive sediments, and (c) uniformly valid for both fine-grained and coarse-grained sediments. Good agreement between this latter equation for natural sediments, the previous equations (when they are valid), and experimental data on quartz particles was demonstrated.

For fine-grained cohesive sediments, the equation for erosion rates can be written as

$$E = 10^{-4}\left(\frac{\tau}{\tau_c}\right)^n \tag{2.4}$$

where τ_c is a function of the sediment bulk density (compare Eq. (2.1)). For non-cohesive sediments, a generally accepted equation is

$$E = A(\tau - \tau_c)^n \tag{2.5}$$

where A is a constant.

In order to approximate the experimental data for all ranges of particle size, the following equation was proposed:

$$E = 10^{-4}\left(\frac{\tau-\tau_{cn}}{\tau_c-\tau_{cn}}\right)^n \tag{2.6}$$

where τ_c, τ_{cn} (critical shear stress for non-cohesive particles), and n are functions of particle diameter. The above equation reduces to Eq (2.4) as particle diameter approaches 0 and to Eq (2.5) for large diameters.

3 EXPERIMENTAL PROCEDURES AND SEDIMENT PROPERTIES

The information in this section is partially based on the articles by McNeil et al. (1996), Taylor and Lick (1996), and Jepsen et al. (1997) and is presented here for completeness.

3.1 Description of Sedflume

Sedflume is shown in Fig. 3.1, and is essentially a straight flume that has a test section with an open bottom through which a rectangular cross-section coring tube containing sediment can be inserted.

The main components of the flume are the coring tube; the test section; an inlet section for uniform, fully developed, turbulent flow; a flow exit section; a water storage tank; and a pump to force water through the system. The coring tube, test section, inlet section, and exit section are made of clear acrylic so that the sediment-water interactions can be observed. The coring tube has a rectangular cross-section, 10 cm by 15 cm, and can be up to 1 m in length.

Water is pumped through the system from a 120 gallon storage tank, through a 5 cm diameter pipe, and then through a flow converter into the rectangular duct shown.

This duct is 2 cm in height, 10 cm in width, and 120 cm in length; it connects to the test section, which has the same cross-sectional area and is 15 cm long. The flow converter changes the shape of the cross-section from circular to the rectangular duct shape while maintaining a constant cross-sectional area. A gate valve near the pump discharge and a ball valve downstream of the exit section regulate the flow. The test section is vented to the atmosphere with a standpipe between the test section and the exit section. The ball valve is throttled as needed at higher flow rates to keep the pressure in the duct and over the test section near atmospheric pressure.

At the start of each test, the coring tube is generally filled with either reconstructed or undisturbed sediments from the bottom of the body of water of interest, or from purchased sediment samples of known composition. In the present tests, mined and graded quartz of known size distribution was used to construct cores. Bulk properties of the quartz will be presented below. The coring tube and the sediment it contains are then inserted into the bottom of the test section. An operator moves the sediment upward using a piston that is inside the coring tube and is connected to a hydraulic jack with a 1 meter long drive. The jack is driven by the release of pressure that is regulated with a switch and valve system. By this means, the sediments can be raised and made level with the bottom of the test section. The speed of the jack can be controlled at a variable rate to produce core movements as small as 0.5 mm.

Water is forced through the duct and the test section over the surface of the sediments. Obtaining a stable flowrate was a prerequisite to starting the erosion

measurement. The shear produced by this flow causes the sediments to erode. Flow rate is measured by an Omega paddlewheel flowmeter, accurate to within 2%. As the sediments in the core erode, they are continually moved upwards by the operator so that the sediment-water interface remains level with the bottom of the test and inlet sections. The erosion rate is recorded as the upward movement of the sediments in the coring tube over time.

Sedflume was modified to allow tilting in the roll and pitch directions. For roll angles, two chains were attached to the side of the frame supporting the inlet, outlet, and test sections of the flume, and the hydraulic jack. The chains were attached to a rope and pulley system that was hooked to the ceiling of the lab. Sedflume was then lowered from its upright position and a clinometer measured the roll angle. Similar methods were used to change the pitch angle of Sedflume. In this case, the chains were attached to the ends of the frame and one end was hoisted upward to change the pitch angle. Sedflume was vented to remove air pockets each time the device was repositioned to prevent inaccurate flow measurements.

3.2 Hydrodynamics

Turbulent flow through pipes has been studied extensively, and empirical functions have been developed which relate the mean flow rate to the wall shear stress. In general, flow in circular cross-section pipes has been investigated. However, the relations developed for flow through circular pipes can be extended to non-circular cross-sections by means of a shape factor. An implicit formula relating the wall shear stress to the mean flow in a pipe of arbitrary cross-section can be

obtained from Prandtl's Universal Law of Friction (Schlichting, 1979). For a pipe with a smooth surface, this formula is

$$\frac{1}{\sqrt{\lambda}} = 2.0 \log\left[\frac{UD\sqrt{\lambda}}{\nu}\right] - 0.8 \tag{3.1}$$

where U is the mean flow speed, ν is the kinematic viscosity, λ is the friction factor, and D is the hydraulic diameter defined as the ratio of four times the cross-sectional area to the wetted perimeter. For a pipe with a rectangular cross-section, or duct, the hydraulic diameter, D, is

$$D = 2hw/(h + w) \tag{3.2}$$

where w is the duct width and h is the duct height. The friction factor is defined by

$$\lambda = \frac{8\tau}{\rho_w U^2} \tag{3.3}$$

where ρ_w is the density of water and τ is the wall shear stress. Inserting Eqs. (3.2) and (3.3) into Eq. (3.1) then gives the wall shear stress τ as an implicit function of the mean flow speed U. Fig. 3.2 shows the relation between shear stress and flow rate.

For shear stresses in the range of 0.1 to 10 N/m^2, the Reynolds numbers, UD/ν, are on the order of 10^4 to 10^5. These values for Reynolds numbers are sufficient for turbulent flow to exist for the stresses of interest in this study. For flow in a circular pipe, turbulent flow theory suggests that the transition from laminar to turbulent flow occurs within 25 to 40 diameters from the entrance to the pipe. Since the diameter of the circular pipe is 5 cm, this suggests an entry length of 125 to 200 cm. The length of the duct leading to the test section is 120 cm and is preceded by a 30 cm flow

$\lambda = \frac{\tau}{\rho} \left[\frac{\lambda}{\nu} \right] -$

converter and several meters of inlet pipe. In addition, since the duct is rectangular with an aspect ratio of five and a hydraulic diameter of 3.3 cm, the transition to turbulence is more rapid than for a circular pipe, probably in as little as 75 cm. These arguments along with direct observations using a dye injector indicate that the flow is fully turbulent in the test section.

Tilting the flume had no effect on the flow rate as long as no air pockets developed in the conduit.

3.3 Sample Preparation

The quartz selected for the present study was obtained from AGSCO Corporation and consisted of 99.5 % silicon dioxide with trace amounts of other metallic oxides. The grain shape was angular for all sizes except for the 5 μm particles which were well-rounded crystalline platy discs. Specific gravity of the material was 2.65 g/cm^3 with a loose pack bulk density in air of 1.23 g/cm^3 for all sizes except for the 5 μm which was 1.28 to 1.36 g/cm^3. The organic content of the material was approximately 0.1 % for all sizes except for the 5 μm which contained approximately 0.19 %. The mean particle diameters used for erosion measurements in the study were 5, 48, 75, 100, 140, 160, 280, and 1350 μm. Fig. 3.3 shows the particle size distribution for these materials. The particle size distributions were measured by means of a Malvern Particle Sizer after thorough disaggregation of any flocculated sediments in a Waring blender. The Wentworth scale, which classifies sediment sizes in terms of clay, silt, and sand, etc., is shown in Table 3.1 for reference.

Sediment cores were prepared as follows. Each sediment was placed in a cylindrical container and mixed with water for 15 to 30 minutes until the sediment-water mixture was homogeneous. The amount of water added was enough to allow the mixture to be fluid, but care was taken to also keep the mixture thick so that stratification of the sediment due to differential settling of the particles was minimized. The sediment mixtures were then poured into coring tubes to a depth of 20 to 50 cm. These cores were then allowed to consolidate for 3, 10, or 64 days. During the consolidation period, sediment particles gradually migrate downward while entrapped air and water migrate to the surface, thus increasing the sample's bulk density over time.

3.4 Sediment Bulk Properties

Bulk densities of the sediments were measured non-destructively as a function of depth by means of the Density Profiler (Gotthard, 1998). The Density Profiler uses a gamma radiation emitter, ^{137}Cs, as a source and measures the attenuation of the radiation as it is transmitted horizontally through the sediments. Once the transmitted radiation is measured, the density of the sediments in the core can be determined from

$$N = N_0 e^{-\mu\rho x} \tag{3.4}$$

where N = number of counts that pass through the core sample; N_o = number of counts with no sample; μ = mass absorption coefficient; ρ= bulk density; and x = sample width (10 cm). By solving for ρ, one obtains

$$\rho = -\frac{1}{\mu x}\,\ell n\,\frac{N}{N_o} \qquad (3.5)$$

For ^{137}Cs and for the present apparatus, μ was determined to be 0.0755 cm^2/g.

The Density Profiler measures the amount of horizontally transmitted radiation as the ^{137}Cs source traverses the core in a vertical direction. For the present set of measurements, this traverse speed was set at 3.3×10^{-3} cm/s (2 mm/min). A rate meter gives an output in counts per minute every 2 s. Because of statistical fluctuations of the radiation, this output is averaged over time (or distance traversed). For most of the data presented here, the data has been averaged over 1 cm in order to reduce the fluctuations in the data and also to illustrate trends more simply.

Particle sizes and particle size distributions were determined by use of a Malvern Particle Sizer for particle diameters between 0.5 and 600 μm. A small amount of quartz was mixed with water and disaggregated in a Waring blender. Approximately 1 mL of this solution was then used for analysis by the particle sizer. From these measurements, the distributions of grain sizes were obtained. The Malvern divides the sediments into 32 different size classes divided logarithmically between 0.5 and 600 μm. To incorporate particles larger than 600 μm into the mean particle diameter, a different lens configuration was used which allowed size measurements ranging from 2 to 2000 μm.

$\rho = -\quad \ell$
μ

3.5 Sediment Erosion Rates

The procedure for measuring the erosion rates of the sediments as a function of shear stress and depth was as follows. The sediment cores were obtained as described above and then moved upward into the test section until the sediment surface became even with the bottom of the test section. A measurement was made of the depth to the bottom of the sediment in the core. The flume was then run at a specific flow rate corresponding to a particular shear stress (see Fig. 3.2). Erosion rates were obtained by measuring the remaining core length at different time intervals, taking the difference between each successive measurement, and dividing by the time interval.

For non-zero roll angles, the sediment was flush with the bottom of the test section for all sediments. For non-cohesive sediments, the roll angles did not exceed the angle at which the sediments slumped due to gravity. For cohesive sediments at angles above the critical angle (the angle of the bed surface at which the bulk material slumps under the influence of gravity), the slump occurred so slowly that the measurements could be taken before the slump affected the core geometry.

In order to measure erosion rates at several different shear stresses using only one core, the following procedure was generally used. Starting at a low shear stress, the flume was run sequentially at higher shear stresses with each succeeding shear stress being twice the previous one. Four shear stresses were run sequentially. Each shear stress was run until at least 2 to 3 mm but no more than 2 cm was eroded. The time interval was recorded for each run with a stopwatch. The flow was then increased to the next shear stress, and so on until the highest shear stress was run. This cycle was

repeated until all of the sediment had eroded from the core. If, after three cycles, a particular shear stress showed a rate of erosion less than 10^{-4} cm/s, it was dropped from the cycle; if after many cycles the erosion rates decreased significantly, a higher shear stress was included in the cycle. Erosion rate measurements are reproducible within ±25% (Roberts et al, 1998).

4 RESULTS AND DISCUSSION

4.1 Erosion Rates as a Function of Pitch Angle

Pitch angle is defined as positive for uphill flows and negative for downhill flows. In the present experiments, erosion rates were measured as a function of pitch angle (from -30˚ to +25˚), for a range of shear stresses (generally 0.4, 0.8, 1.6, and 3.2 N/m^2), and for a range of particle sizes and consolidation times. For a consolidation time of 3 d, particle sizes were 1350, 280, 160, 48, and 5-µm. For a consolidation time of 10 d, particle sizes were 1350, 280, 100, 48, and 5-µm. For a consolidation time of 64 d, experiments were only done for a particle size of 280-µm.

For a consolidation time of 3 d, erosion rates as a function of pitch angle with shear stress as a parameter are shown for different particle sizes in Figs. 4.1 a-e. For 1350-µm (Fig. 4.1a), erosion rates were minimum at zero angle and increased for both negative (downhill) and positive (uphill) angles. As an example, the erosion rate for the 48 µm sample at 3.2 N/m^2 was .07 cm/s at 25°, decreased to a value of .02 cm/s at zero angle, and then increased to a value of nearly 0.1 cm/s at 30° (Fig. 4.1d).

Erosion rates generally increased more rapidly as a function of slope angle for downhill flows than for uphill flows. For uphill flows, and at 0.4 and 0.8 N/m^2, it was observed that particles slowly crept uphill; at lower values of the shear stress just above critical, the suspended particles hardly moved. This resulted in erosion rates which were nearly the same at low positive angles as for zero angles. For negative angles, particles moved downwards more rapidly as the pitch angle became more negative.

Erosion rates for 280-μm (Fig. 4.1b) are qualitatively similar to those for 1350-μm. However, as particle size decreases further (compare Figs. 4.1 a-e), (1) erosion rates decrease and (2) the effect of pitch angle (magnitude of change in erosion with pitch angle) generally decreases, for both positive and negative angles. Both of these effects are due to cohesive forces which become more important relative to gravitational forces (see Fig. 2.1) as particle size decreases. For the smallest particles, cohesive forces are much greater than gravitational forces and, in the limit as $F_c >> F_g$, erosion rates should be independent of pitch angle (either positive or negative) as they almost are for 48 and 5-μm (Figs. 4.1 d and e) (Note changes in scales).

For consolidation times of 10 d, (Figs. 4.2 a-e), the results are qualitatively the same. However, because the sediments have consolidated for a longer time, erosion rates are either the same or lower than for a consolidation time of 3 d. For a particle size of 1350-μm, comparison of Fig. 4.2a with Fig 4.1a indicates that erosion rates are similar. For 1350-μm, cohesive forces are negligible compared to gravitational forces. Because of this, sediments do not compact readily and erosion rates remain

unchanged. Within experimental error, erosion rates are also unchanged for 280-µm at 3 d and 10 d. For 48 and 5-µm, effects of consolidation are evident (compare Figs. 4.2d and e with Figs. 4.1d and e). In these cases, cohesive forces are greater than gravitational forces and increase as consolidation (bulk density) increases. Because of this, erosion rates decrease.

For a particle size of 280-µm and a consolidation time of 64 d, erosion rates are shown as a function of pitch angle in Fig. 4.3. By comparison with Fig 4.1b, it can be seen that consolidation effects are significant and erosion rates have been reduced.

4.2 Erosion Rates as a Function of Roll Angle

In these experiments, erosion rates were measured as a function of roll angle (from 0 to as high as 75˚), for a range of particle sizes (1350, 280, 160, 140, 100, 75, 48, and 5-µm), and a range of shear stresses (0.4, 0.8, 1.6, and 3.2 N/m^2). Consolidation times were 3 d for the medium and coarse sediments (1350, 280, 160, 140, and 100-µm), but were 10 d for the fine sediments with mean diameters of 75, 48, and 5-µm.

Erosion rates as a function of roll angle with shear stress as a parameter are shown in Figs. 4.4 a-h. For most particles, erosion rates increased as a function of roll angle and as a function of shear stress with the increases being greater for the coarser particles. The erosion rate of the 1350 µm sample changed by three orders of magnitude as the shear stress was increased from 0.4 N/m^2 to 3.2 N/m^2 and the erosion rate of the 5 µm sample changed from approximately .001 cm/sec at 0.8 N/m^2

to approximately .02 cm/sec at 3.2 N/m^2. The results at zero roll angle are consistent with those of Roberts et al., 1998.

For 280-µm, the variations are similar to those for 1350-µm. However, as the particle size decreases, the dependence of erosion rate on both the shear stress and roll angle decreases. For 75-µm, erosion rates are almost independent of roll angle for all angles up to 75˚.

For 48 and 5-µm, erosion rates are practically independent of angle. However, results for these smaller sizes can not be compared quantitatively with those for the larger sizes since the smaller sized sediments have consolidated for a longer time (10 d) than those for the larger sizes (3 d). Nevertheless, the qualitative result that the dependence of erosion rate on roll angle decreases as particle size decreases is correct. The reason for this is that, as particle size decreases, cohesive forces become much greater than gravity forces (just as in the pitch angle experiments), and the relative effects of gravity therefore decrease.

4.3 Effects of the Addition of Fine-Grained Particles

Experiments were also conducted to further investigate the effects of cohesive forces. This was done by adding a small amount (5%) of fine-grained (20-µm) sediment to 160-µm sediment and performing experiments to determine erosion rates as a function of roll angle. The particle size distribution for this sediment, before and after adding fine particles, is shown in Fig. 4.5. For the 160-µm sediment (without fines), erosion rates are shown in Fig. 4.4c. The erosion rate is almost independent of angle for small angles, but increases rapidly near a roll angle of 35˚. By contrast,

erosion rates for the 160-μm sediment with 5% added fines (Fig. 4.6) are somewhat lower and are low and independent of angle for all angles up to 60˚.

4.4 Critical Angle Measurement

The critical angle is defined as the angle of the bed surface at which the bulk material slumps under the influence of gravity. This angle was measured for seven different-sized particles.

To measure critical angle, samples of sediment were placed in standard core tubes and filled with water. Samples of 15, 48, 75, 100, 160, 400, and 1350-μm were available. Particle size distributions are shown in Fig. 4.7. The 1350-μm sample was consolidated for 3 days. One sample of each of the other sizes was consolidated for 3 days and another for 10 days. Each sample holder was tilted until the surface particles began to slide under the influence of gravity. The angle at which this occurred was termed the critical angle. Measurement results are shown in Table 4.1. It is worth noting that all of the samples, whether consolidated for 3 or 10 days, showed some slumping of what can be called "soft surface material." This material was a mixture of water and very fine particles (measured in the Malvern particle sizer in the 10-μm range) that slumped at smaller angles than the bulk of the material and had equilibrium slopes of between 0 and about 15˚.

After 3 days of consolidation, all of the samples slumped at critical angles ranging from 44˚ for 1350-μm to 65˚ for the 15-μm sediment. The resulting surface profile for each of these was curved when viewed from the side. The 15-μm sediment

behaved differently from the others. Instead of slumping at 65˚, the bulk material pulled away from the wall of the sample holder and an 8 mm thick layer of sediment failed in shear, with the sediment below it slumping slowly over time. At 70˚, another layer, 25 mm thick, failed in shear.

The 10-day samples showed distinct effects of consolidation. While there was some slumping of soft surface material, the bulk material of the sediments below 160-µm did not slump. The 15-µm sample once again experienced a shear failure; however, it did not occur until two hours after the sample was tilted to 90˚. The surface profile of the 400-µm sample was similar to the profile of the 3 d sample, but all other samples had vertical or near vertical bed surfaces (with the sample holders tilted to 90˚), and a thin layer of soft surface material that slumped to equilibrium slopes of between 0 and about 15˚.

The measurements reinforced the observation that cohesive effects are increasingly important as particle size decreases and that increased consolidation time affects the critical angle and is more important as particle size decreases.

5 SUMMARY AND CONCLUDING REMARKS

The effects of surface slope on erosion rates of quartz particles were investigated. Erosion rates were measured for quartz particles with mean diameters of 5 to 1350-µm, applied shear stresses of 0.4 to 3.2 N/m^2, pitch angles from -30 to +25˚, and roll angles from 0 to 75˚. The sediments consolidated for 3 d, 10 d, or 64 d.

Erosion rates increased for both increasing negative and positive pitch angles. The increase was more rapid as a function of pitch angle for downhill flows than for uphill flows. As particle size decreased below 280-µm, (1) erosion rates decreased and (2) the effect of pitch angle decreased.

Roll angle measurements produced qualitatively similar results, i.e., as particle size decreased below 280-µm, the dependence of erosion rate on roll angle decreased as particle size decreased.

Reduced effects on erosion rates as a function of pitch and roll angles as particle size decreases can be explained by cohesive forces that become dominant over gravitational forces as particle size decreases. For the smallest particle sizes, $F_c >> F_g$, and erosion rates should be independent of pitch angle, as they almost were for 48 and 5-µm particles.

Increased consolidation time served to reduce erosion rates, due to higher bulk density.

Experiments were also conducted by adding 5% of 20-µm quartz to 160-µm quartz. By comparison with 160-µm sediment, with very few silt and clay particles, the mixed sediment behaved as a cohesive sediment similar in character to the smaller particles, with roll angle having little effect on erosion rates (compare Figs. 4.4c and 4.5).

The critical angle of several quartz sediments in the general size range used in the erosion experiments was measured. The cohesive effects seen in the erosion experiments were also present when measuring critical angle, causing the smaller

particles to have greater resistance to surface movement caused by gravity. The measurements reinforced the observation that cohesive effects are increasingly important as particle size decreases and that increased consolidation time increases the critical angle and is more important as particle size decreases.

Surface slope was shown to affect erosion rates of quartz particles, with a general tendency to increase erosion with surface slope (either pitch or roll), but there is a decreasing effect as particle size decreases, due to the increased importance of cohesive forces compared to gravitational forces. The quantitative results of these experiments are limited to quartz sediments with the particle sizes and distributions used in these experiments and to similar consolidation times. Forecasting the effect of bed slopes on erosion in natural sediments under different conditions than these could be problematic, because of the complex interactions of particle size and size distribution, consolidation time, and other parameters. For example, the addition of fine particles, in this study, to a sample with a fairly narrow particle-size distribution dramatically altered the behavior of the sediment bed. (Much more extensive experiments with additions of fines to study their effects on erosion behavior can be found in Jin et al, 2000).

As stated earlier in this paper, prior research on erosion in natural sediments has qualitatively determined that erosion rates depend on at least the following parameters: bulk density, particle size (mean and distribution), mineralogy, organic content, salinity of the pore water, amount of gas, oxidation or other chemical reactions, and consolidation time. Sediment bed slope can be added to this list. For

the purposes of understanding and accurately predicting erosion rates, the dependence of erosion rates on these parameters needs to be known. Extending the results of this study to natural sediment beds, with infinitely variable particle size distributions, and adding the complexities of organic and other impurities, mineralogy, salinity, etc., the ability to predict the effect of slope on natural sediment bed erosion is questionable without further study.

6 REFERENCES

Chepil, W.S., 1959. "Equilibrium of Soil Grains at the Threshold of Movement by Wind," Soil Sci. Soc. Proc., 23, pp. 422-428

Damgaard, J. S., Whitehouse, R. J. S., and Soulsby, R.L., 1997, "Bed-Load Sediment Transport on Steep Longitudinal Slopes," Journal of Hydraulic Engineering, December 1997, pp. 1130-1138

Fukuda, M. and W. J. Lick, 1980. "The Entrainment of Cohesive Sediments in Freshwater," J. geophysical Research, V85, pp. 2813-2824

Gailani, J., Jin, L., and Lick, W, 2004. Initiation of Movement of Quartz Particles. Report, Department of Mechanical and Environmental Engineering, University of California, Santa Barbara, CA 93106.

Gessler, J., 1965. "The Beginning of Bedload Movement of Mixtures Investigated as Natural Armoring in Channels," Laboratory of Hydraulic Research and Soil Mechanics, Swill Federal Institute of Technology, Report No. 69

Gotthard, D., 1998. Three-Dimensional, Non-Destructive Measurements of Sediment Bulk Density Using Gamma Attenuation. Report, Department of Mechanical and Environmental Engineering, University of California, Santa Barbara, CA 93106.

Jepsen, R., J. McNeil, and W. Lick, 1999. Effects of gas generation on the density and erosion of sediments from the Grand River, J. Great Lakes Res. 26(2), pp. 209-219.

Jepsen, R., J. Roberts, and W. Lick, 1997. Effects of bulk density on sediment erosion rates. Water, Air, and Soil Pollution, 99, pp. 21-31.

Jin, L., J. McNeil, and W. Lick, 2000. Effects of Bentonite on Sediment Erosion Rates. Report, Department of Mechanical and Environmental Engineering, University of California, Santa Barbara, CA 93106.

Jones, C., 1999. "An Accurate Model of Sediment Erosion and Transport," Proc. Estuarine and Coastal Modeling, Nov 3-5, 1999 (pending)

McNeil, J., C. Taylor, and W. Lick, 1996. Measurements of erosion of undisturbed bottom sediments with depth. J. Hydr. Engrg., ASCE, 122(6), pp. 316-324.

Mehta, A.J., T .M. Parchure, J .G. Dixit, and R. Ariathuri, 1982. "Resuspension Potential of Deposited Cohesive Beds," Estuarine comparisons, edited by V.S. Kennedy, Academic Press, NY, 99. 591-609

Melville, B.W., and Raudkivi, A.J., "Flow Characteristics in Local Scour at Bridges," Journal of Hydraulic Research, Vol 15, N4, pp. 373-380

Melville, B. W., 1994. "Live-Bed Scour at Bridge Piers," Journal of Hydraulic Engineering, Vol 110, N9, pp .1234-1247

Melville, B. W., 1997. "Pier and Abutment Scour: Integrated Approach," Journal of Hydraulic Engineering, Vol 123, N2, pp. 125-136

Melville, B. W., and Y. Chiew, 1999. "Time Scale For Local Scour at Bridge Piers," Journal of Hydraulic Engineering, Vol 125, Nl, pp. 59-65

Roberts, J., R. Jepsen, D. Gotthard, and W. Lick, 1998. Effects of particle size and bulk density on erosion of quarts particles. J. Hydr. Engr., 124(12), pp. 1261-1267.

Schlichting, H., 1979. Boundary Layer Theory, McGraw-Hill, New York, NY.

Taylor, C. and W. Lick, 1996. Erosion Properties of Great Lakes Sediments. Report, Department of Mechanical and Environmental Engineering, University of California, Santa Barbara, CA 93106.

Tsai, C.H., and W. Lick, 1986. "A Portable Device for Measuring Sediment Resuspension," J. of Great Lakes Research, Vol. 12, No.4, pp. 314-321.

White, S.J., 1970. "Plane Bed Thresholds of Fine-Grained Sediments," Nature, Vol. 228, pp.152-153

Whitehouse, R., 1998. "Scour at Marine Structures," Thomas Telford Publications, Thomas Telford Ltd.

7 TABLES

Wentworth Scale				
		mm	phi units	Microns
	Boulder	>256	<-8	
	Cobble	64 to 256	-6 to -8	
Pebble	Large	32 to 64	-5 to -6	
	Medium	16 to 32	-4 to -5	
	Small	8 to 16	-3 to -4	
	Very Small	4 to 8	-2 to -3	
	Granule	2 to 4	-1 to -2	
Sand	Very Coarse	1 to 2	0 to -1	1000 to 2000-µm
	Coarse	1/2 to 1	1 to 0	500 to 1000-µm
	Medium	1/4 to 1/2	2 to 1	250 to 500-µm
	Fine	1/8 to 1/4	3 to2	125 to 250-µm
	Very Fine	1/16 to 1/8	4 to 3	62.5 to 125-µm
Silt	Coarse	1/32 to 1/16	5 to 4	31.2 to 62.5-µm
	Medium	1/64 to 1/32	6 to 5	15.6 to 31.2-µm
	Fine	1/128 to 1/64	7 to 6	7.81 to 15.6-µm
	Very Fine	1/256 to 1/128	8 to 7	3.91 to 7.81-µm
Clay	Coarse	1/512 to 1/256	9 to 8	
	Medium	1/1024 to 1/512	10 to 9	
	Fine	1/2048 to 1/1024	11 to 10	
	Very Fine	1/4096 to 1/2048	12 to 11	

Table 3.1: The Wentworth Scale

Particle Size (μm)	3 d Critical Angle (deg.)	10 d Critical Angle (deg.)
1350	44	N/A
400	50	45
160	50	50
100	50	90
75	60	90
48	50	90
20	65	90

Table 4.1: Critical Angle Measurement

8 FIGURES

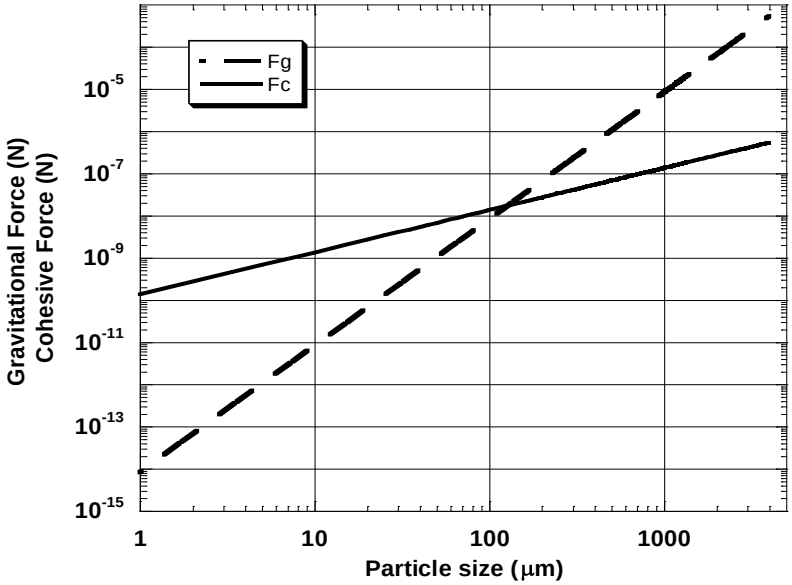

Figure 2.1: Gravitational and Cohesive Forces as a Function of Particle Diameter

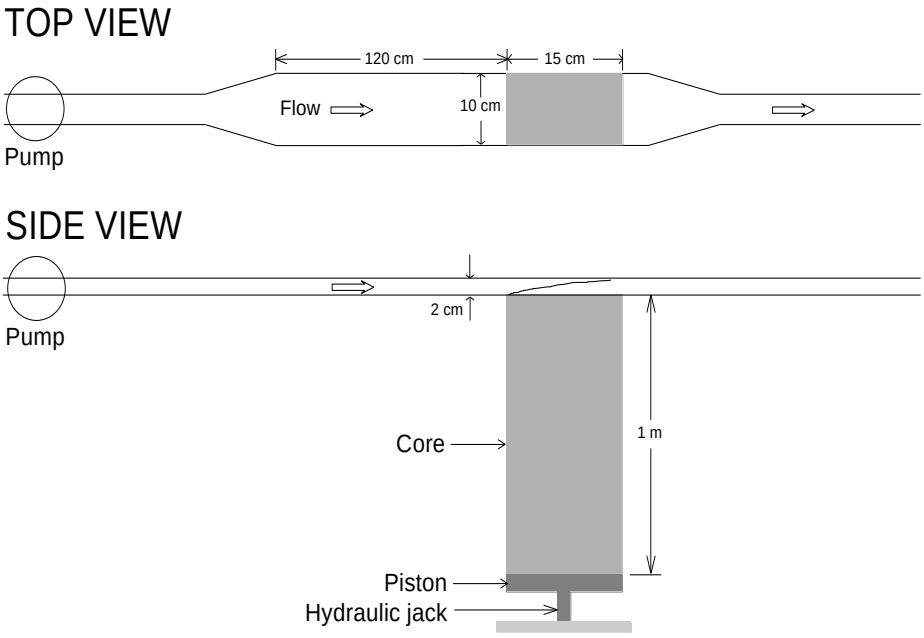

Figure 3.1: Sedflume

μ

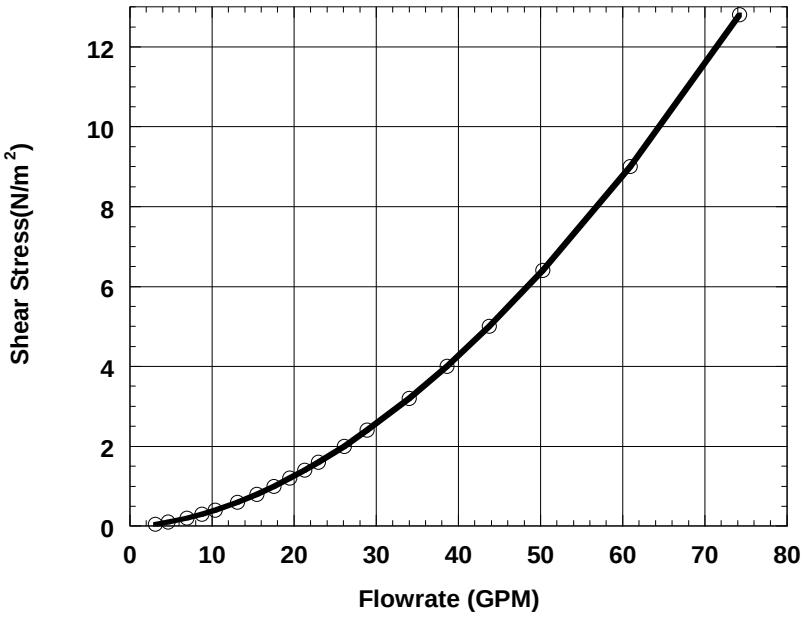

Figure 3.2: Shear Stress(N/m^2)as a Function of Flowrate (GPM) for Sedflume

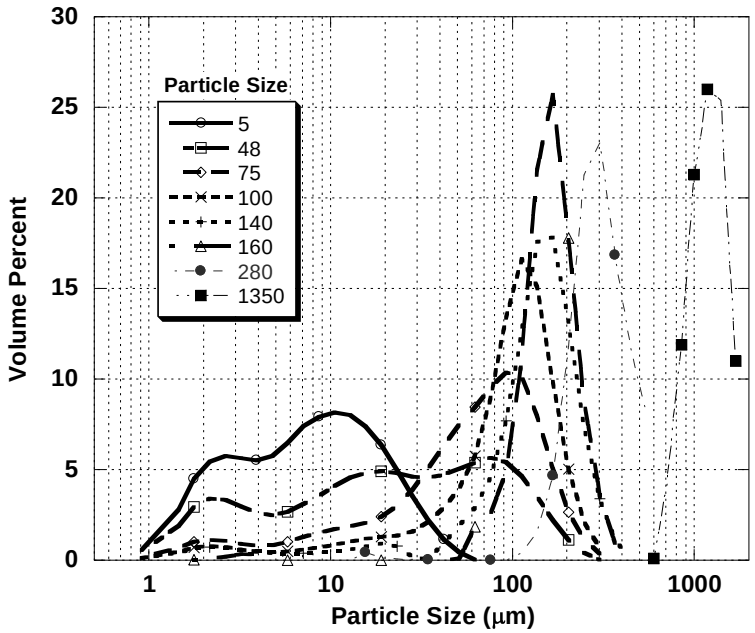

Figure 3.3: Particle Size Distributions of 5, 48, 75, 100, 140, 160, 280, and 1350 μm Quartz.

μ

μ

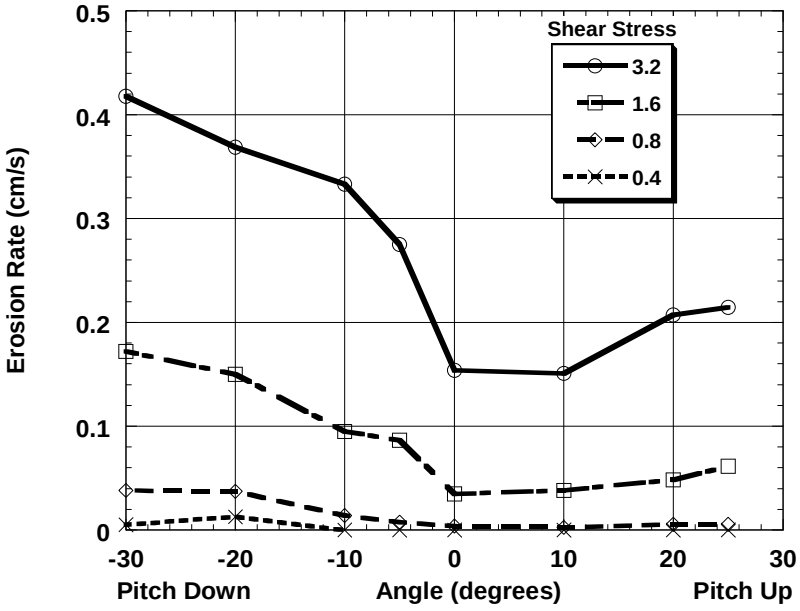

Figure 4.1a: Erosion Rate as a Function of Pitch Angle with Shear Stress (N/m^2) as a Parameter for 1350 μm Quartz. Consolidation time is 3 d.

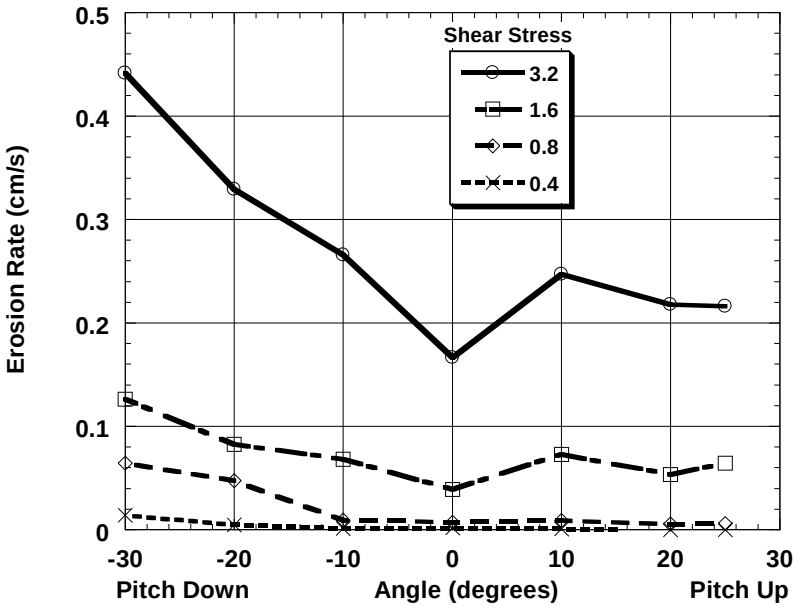

Figure 4.1b: Erosion Rate as a Function of Pitch Angle with Shear Stress (N/m^2) as a Parameter for 280 μm Quartz. Consolidation time is 3 d.

μ

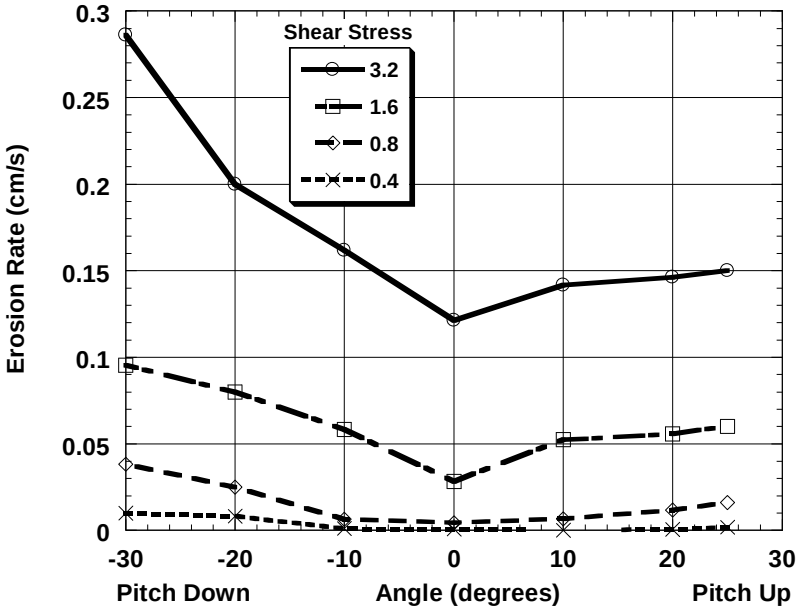

Figure 4.1c: Erosion Rate as a Function of Pitch Angle with Shear Stress (N/m^2) as a Parameter for 160 μm Quartz. Consolidation time is 3 d.

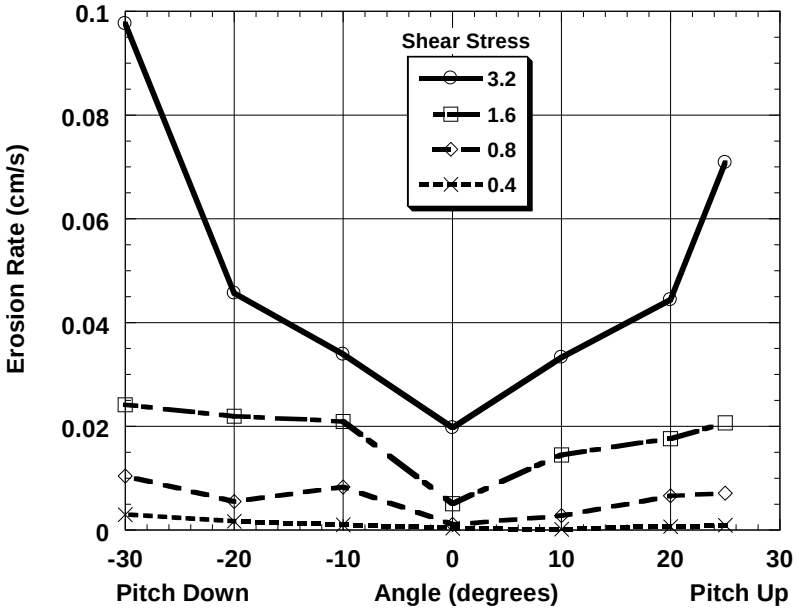

Figure 4.1d: Erosion Rate as a Function of Pitch Angle with Shear Stress (N/m^2) as a Parameter for 48 μm Quartz. Consolidation time is 3 d.

μμ

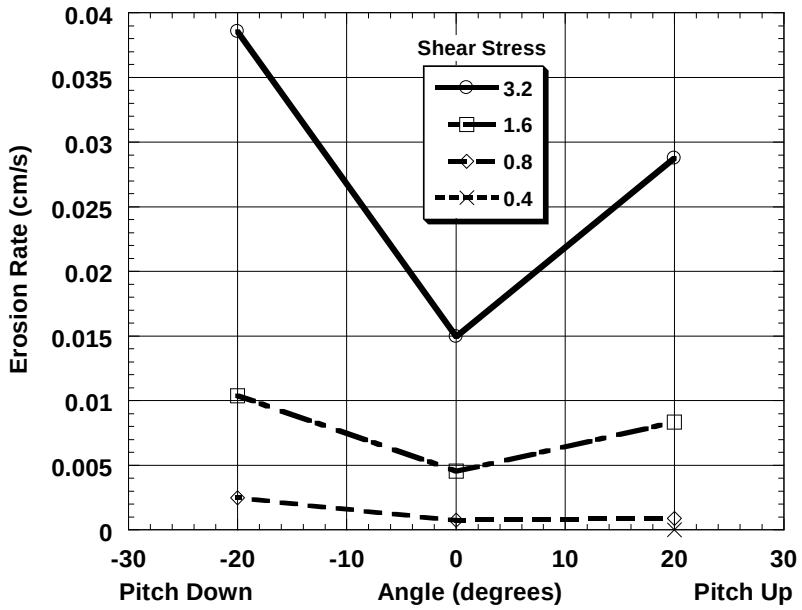

Figure 4.1e: Erosion Rate as a Function of Pitch Angle with Shear Stress (N/m^2) as a Parameter for 5 μm Quartz. Consolidation time is 3 d.

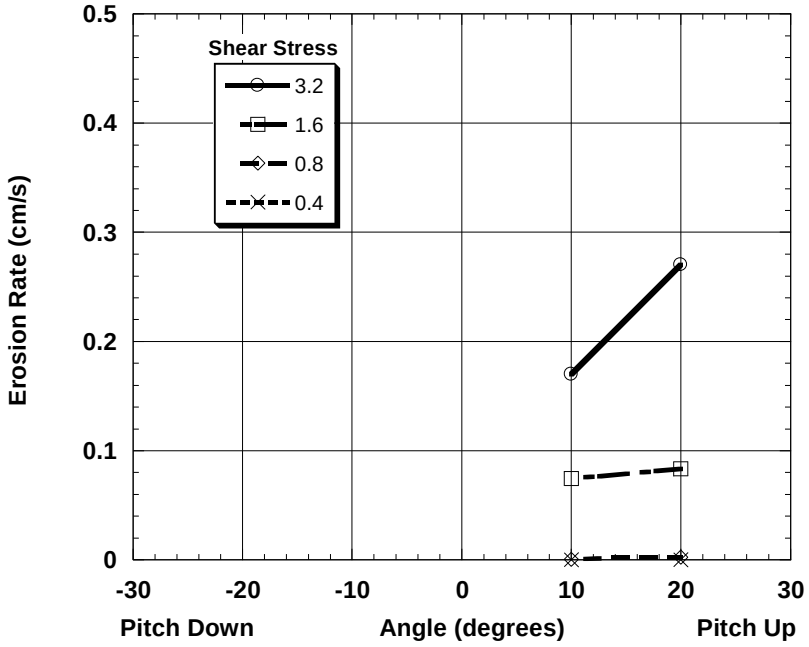

Figure 4.2a: Erosion Rate as a Function of Pitch Angle with Shear Stress (N/m^2) as a Parameter for 1350 μm Quartz. Consolidation time is 10 d.

μ

μ

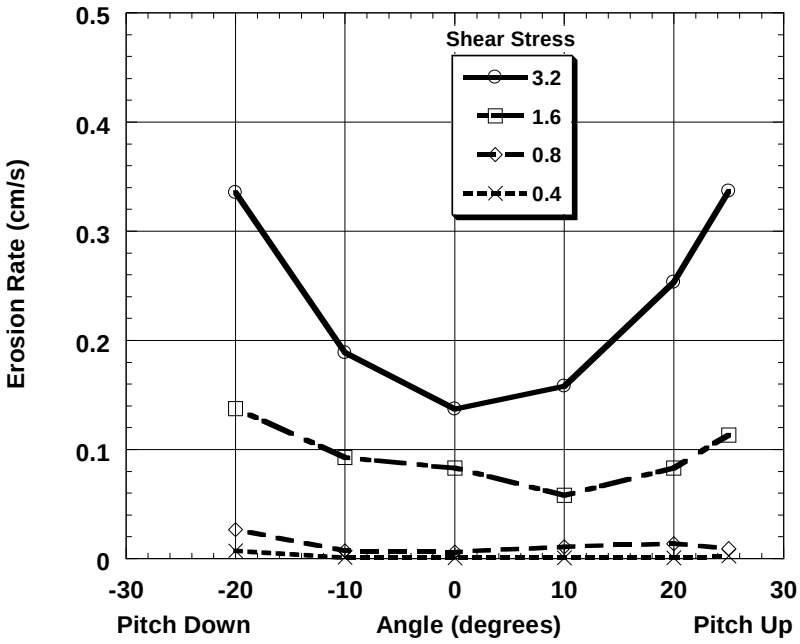

Figure 4.2b: Erosion Rate as a Function of Pitch Angle with Shear Stress (N/m^2) as a Parameter for 280 μm Quartz. Consolidation time is 10 d.

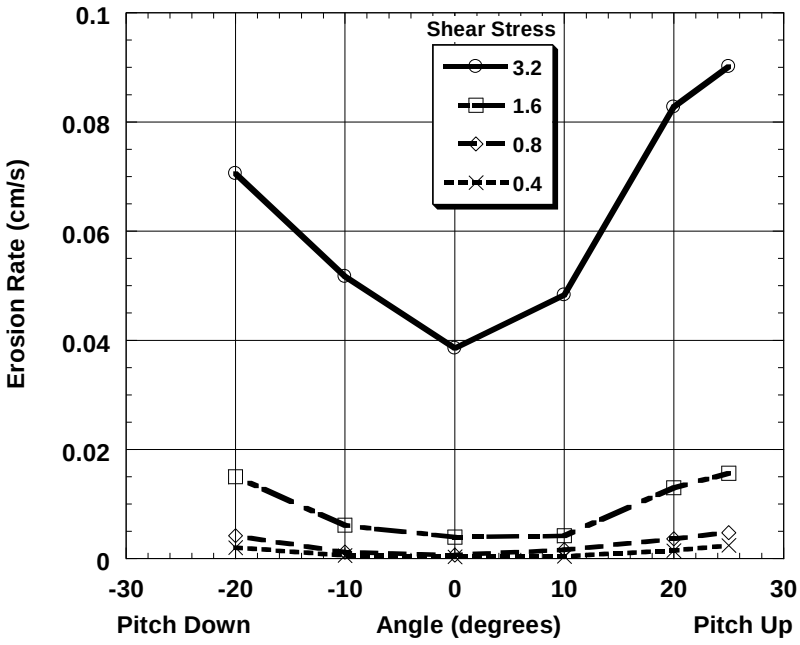

Figure 4.2c: Erosion Rate as a Function of Pitch Angle with Shear Stress (N/m^2) as a Parameter for 100 μm Quartz. Consolidation time is 10 d.

μμ

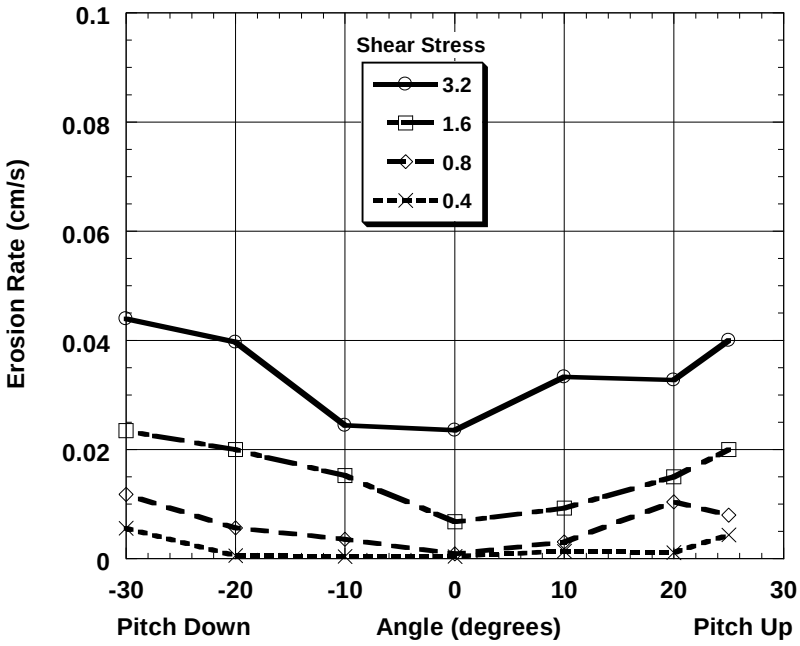

Figure 4.2d: Erosion Rate as a Function of Pitch Angle with Shear Stress (N/m^2) as a Parameter for 48 μm Quartz. Consolidation time is 10 d.

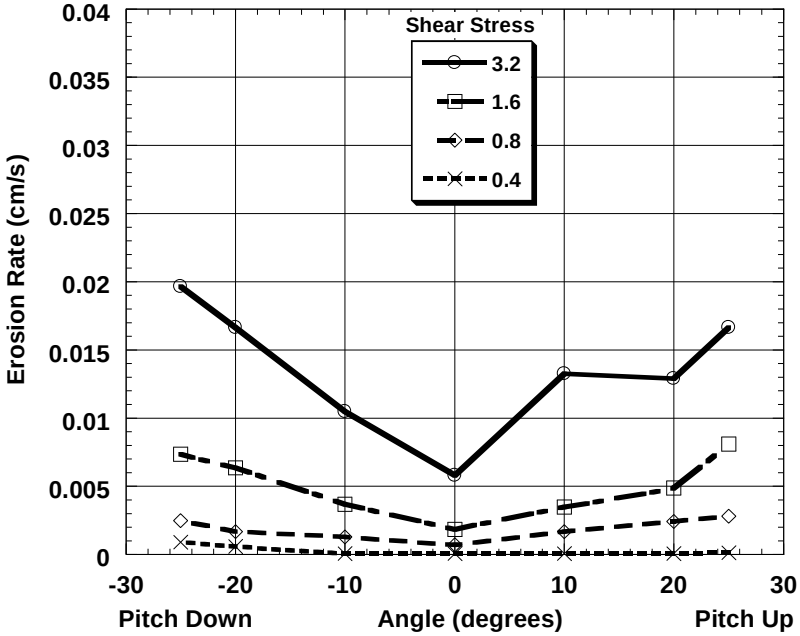

Figure 4.2e: Erosion Rate as a Function of Pitch Angle with Shear Stress (N/m^2) as a Parameter for 5 μm Quartz. Consolidation time is 10 d.

μ μ

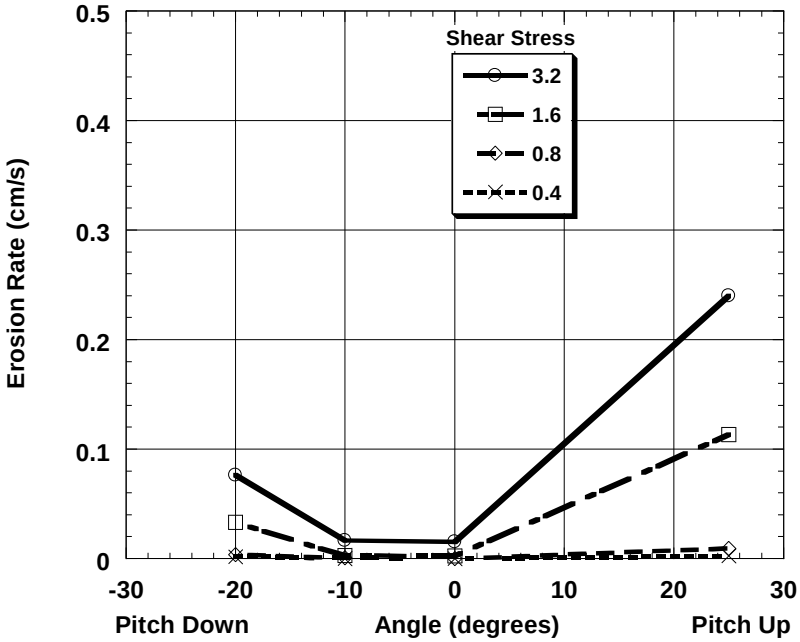

Figure 4.3: Erosion Rate as a Function of Pitch Angle with Shear Stress (N/m^2) as a Parameter for 280 μm Quartz. Consolidation time is 64 d.

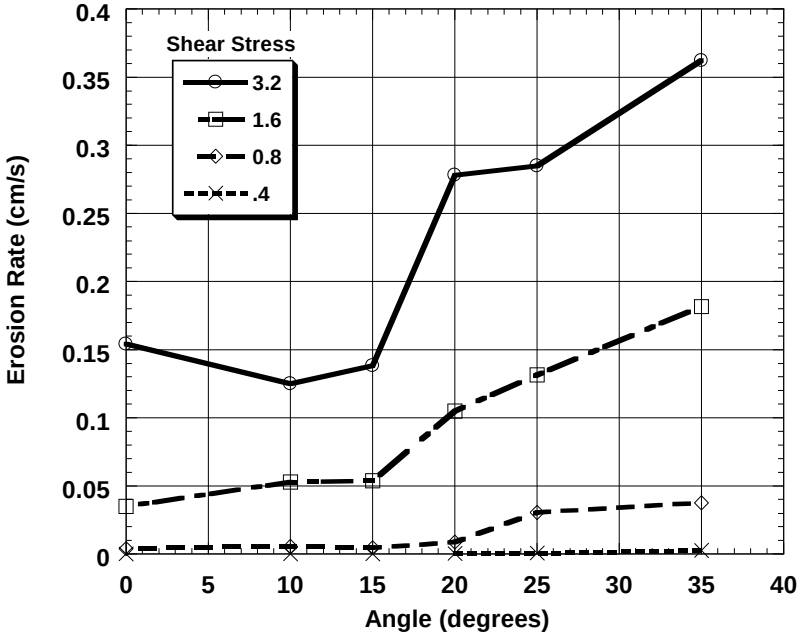

Figure 4.4a: Erosion Rate as a Function of Roll Angle with Shear Stress (N/m^2) as a Parameter for 1350 μm Quartz.

μ μ

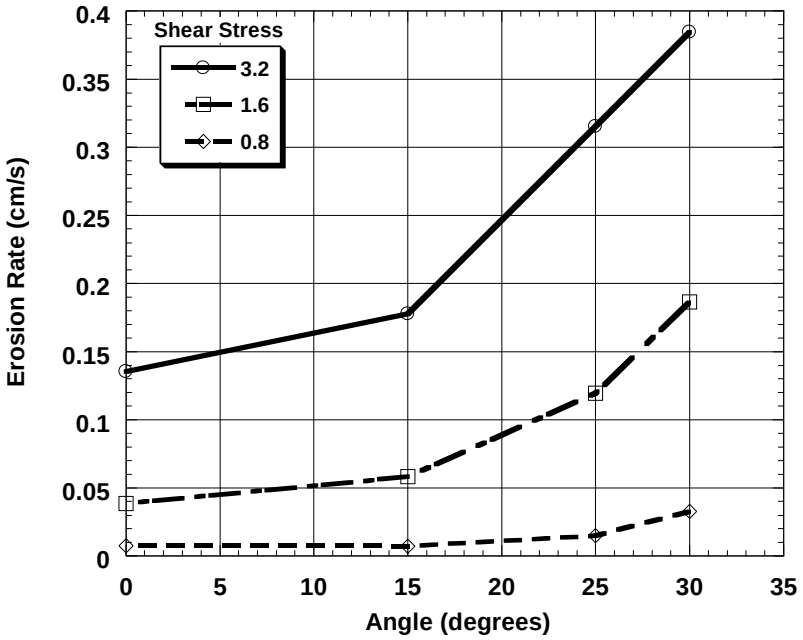

Figure 4.4b: Erosion Rate as a Function of Roll Angle with Shear Stress (N/m^2) as a Parameter for 280 μm Quartz.

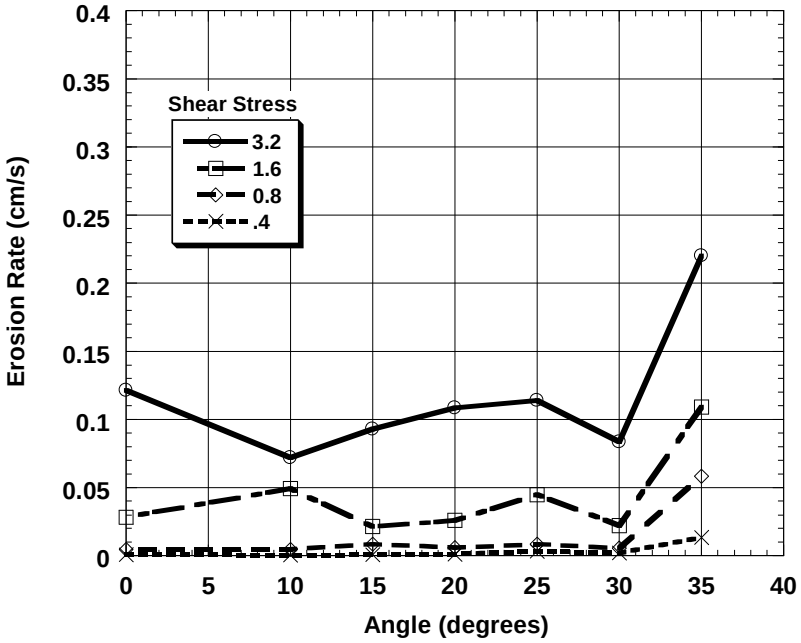

Figure 4.4c: Erosion Rate as a Function of Roll Angle with Shear Stress (N/m^2) as a Parameter for 160 μm Quartz

μμ

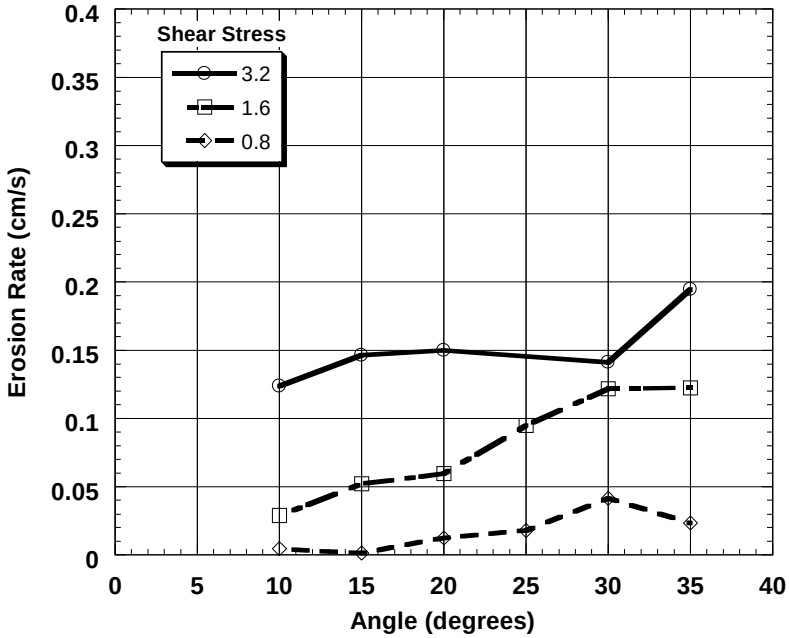

Figure 4.4d: Erosion Rate as a Function of Roll Angle with Shear Stress (N/m^2) as a Parameter for 140 μm Quartz

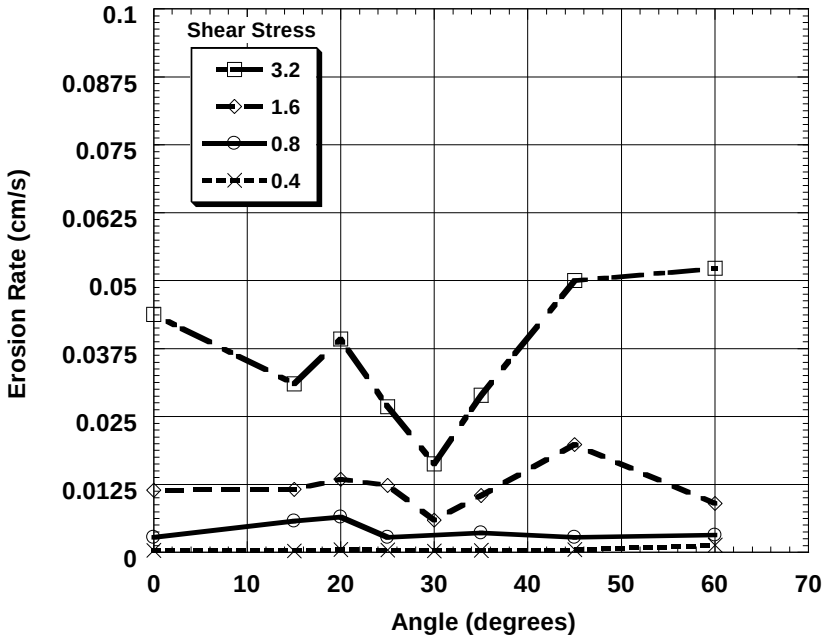

Figure 4.4e: Erosion Rate as a Function of Roll Angle with Shear Stress (N/m^2) as a Parameter for 100 μm Quartz

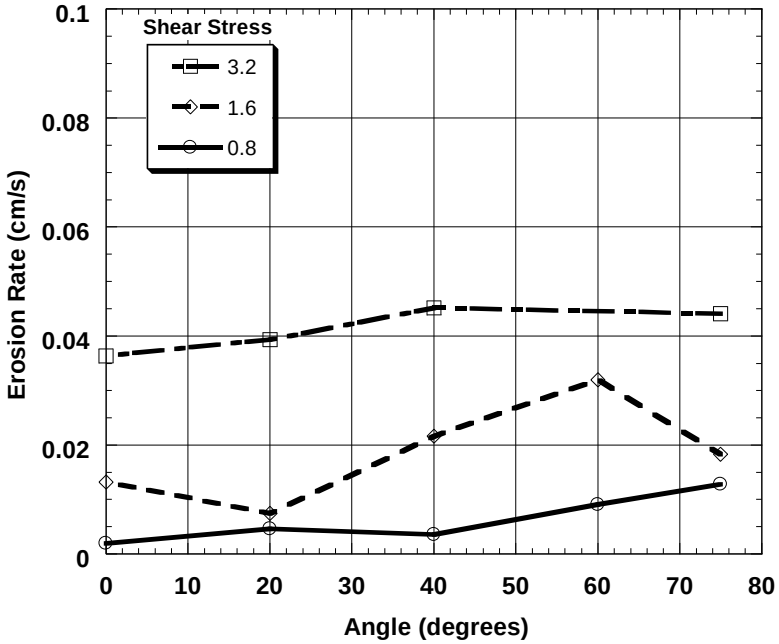

Figure 4.4f: Erosion Rate as a Function of Roll Angle with Shear Stress (N/m^2) as a Parameter for 75 μm Quartz

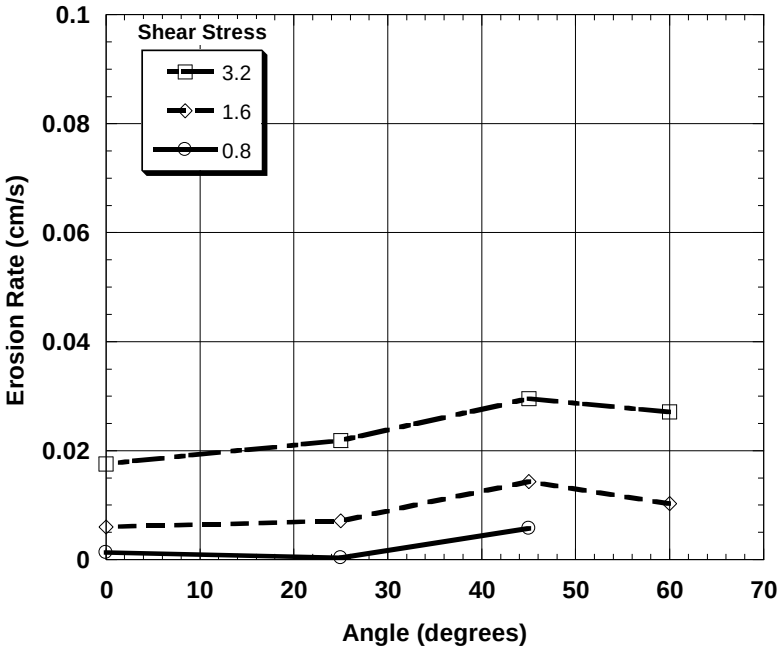

Figure 4.4g: Erosion Rate as a Function of Roll Angle with Shear Stress (N/m^2) as a Parameter for 48 μm Quartz

μμ

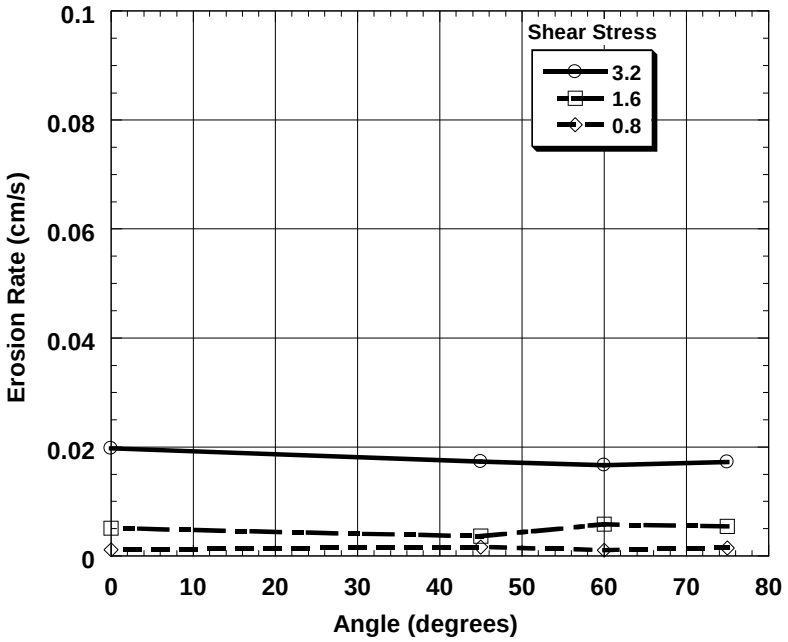

Figure 4.4h: Erosion Rate as a Function of Roll Angle with Shear Stress (N/m^2) as a Parameter for 5 μm Quartz

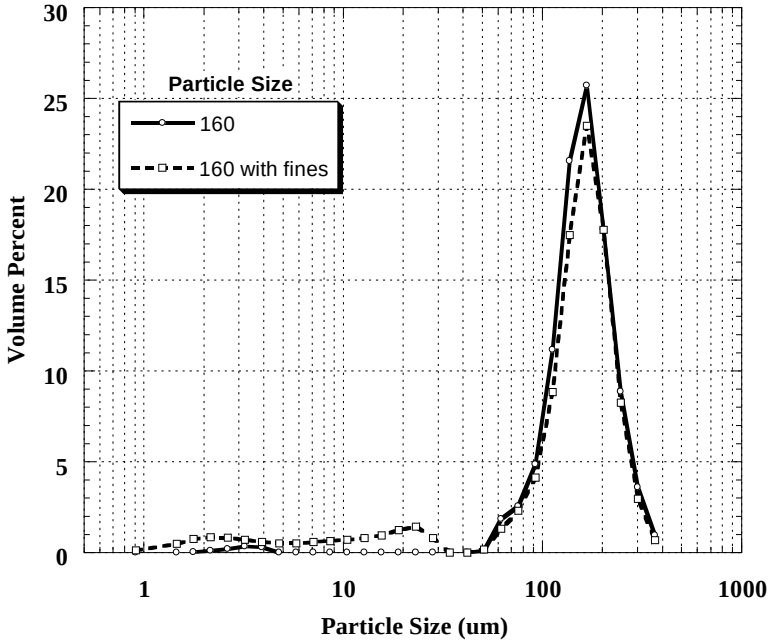

Figure 4.5: Particle Size Distribution for 160 μm Quartz with Added 5.0% 20 μm Quartz.

μ

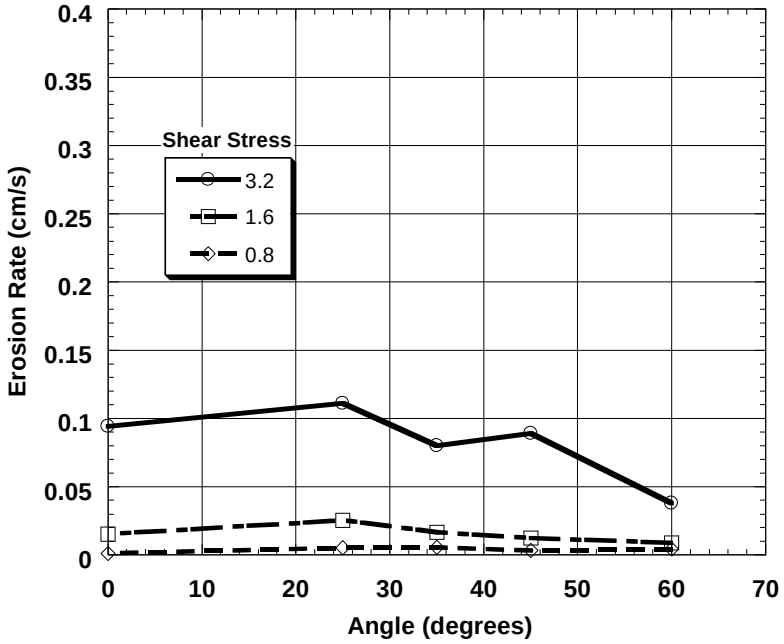

Figure 4.6 Erosion Rate as a Function of Roll Angle with Shear Stress (N/m^2) as a Parameter for 160 μm Quartz with 5.0 % 20 μm Quartz Added.

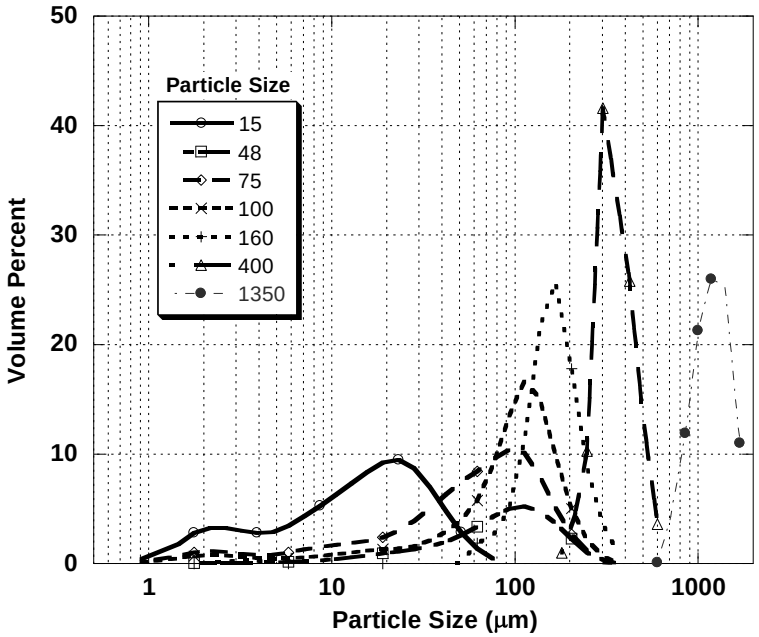

Figure 4.7: Particle Size Distributions of 15, 48, 75, 100, 160, 400 and 1350 μm Quartz.

μ

μ

μ

μ